

# Refined mean field model of heat and momentum transfer in magnetoconvection

Till Zürner\*

*Institut des Sciences de la Mécanique et Applications Industrielles (IMSI),  
ENSTA-ParisTech/CNRS/CEA/EDF/Institut Polytechnique de Paris,  
828 Boulevard des Marechaux, 91120 Palaiseau, France*

(Dated: March 25, 2022)

In this article, the theoretical model on heat and momentum transfer for Rayleigh-Bénard convection in a vertical magnetic field by Zrner *et al.* (Phys. Rev. E **94**, 043108 (2016)) is revisited. Using new data from recent experimental and numerical studies the model is simplified and extended to the full range of Hartmann numbers, reproducing the results of the Grossmann-Lohse theory in the limit of vanishing magnetic fields. The revised model is compared to experimental results in liquid metal magnetoconvection and shows that the heat transport is described satisfactorily. The momentum transport in form of the Reynolds number agrees less well which reveals some shortcomings in the theoretical treatment of magnetoconvection.

## I. INTRODUCTION

Magnetoconvection considers the interaction of magnetic fields with thermal convection flows in electrically conducting fluids. The most notable examples of such systems in nature are liquid iron cores of planets and the plasma inside stars generating global magnetic fields in the so-called dynamo effect [1, 2]. In technological applications, magnetoconvection may be relevant for liquid metal batteries [3] and in proposed liquid metal cooling blankets for fusion reactors [4]. The study of magnetoconvection is numerically and experimentally difficult due to the extreme conditions that often govern these systems. Additionally, the most relevant fluids are liquid metals and plasmas which are either very hard or impossible to handle experimentally. A theoretical understanding of canonical setups is thus important to understand the relevant mechanisms at play and to predict their behavior beyond the currently accessible parameter space.

In a previous article [5], a theoretical model was developed to predict the heat and momentum transfer in a Rayleigh-Bénard convection (RBC) system subject to a vertical magnetic field. It utilized the ansatz by Grossmann and Lohse [6] and incorporated the effect of Joule dissipation induced by the magnetic field. The preceding works of Chakraborty [7] on the same topic should be mentioned here as well. At the time, the study suffered the lack of numerical and especially experimental data which limited a proper evaluation and validation of the theory. However, after a number of new studies have been published on the topic over the past few years the model [5] can be revisited and revised. The aim of the present article is (i) to simplify the existing model by reducing its number of free parameters and reconsidering the validity of the physical mechanisms included and (ii) to extend it to a larger parameter space.

Rayleigh-Bnard convection considers a horizontal fluid layer of height  $H$  heated at its lower boundary and cooled at its upper boundary with constant temperatures  $T_{\text{bot}}$  and  $T_{\text{top}}$ , respectively, where  $T_{\text{top}} < T_{\text{bot}}$ . A fluid with a sufficiently large electrical conductivity  $\sigma$  can be influenced by imposing a magnetic field which in the present case is a homogeneous vertical magnetic field  $\mathbf{B}_0 = B_0 \mathbf{e}_z$  (with the  $z$ -axis in vertical direction). The flow is controlled by five dimensionless parameters

$$\text{Ra} = \frac{g\alpha\Delta TH^3}{\nu\kappa}, \quad \text{Ha} = B_0 H \sqrt{\frac{\sigma}{\rho_0\nu}}, \quad \text{Pr} = \frac{\nu}{\kappa}, \quad \text{Pm} = \frac{\nu}{\eta}, \quad \Gamma = \frac{L}{H}. \quad (1)$$

The Rayleigh number  $\text{Ra}$  quantifies the thermal driving of the fluid by the temperature difference  $\Delta T = T_{\text{bot}} - T_{\text{top}}$  and the Hartmann number  $\text{Ha}$  gives a measure of the magnetic field strength. The fluid is characterized by the thermal Prandtl number  $\text{Pr}$  and the magnetic Prandtl number  $\text{Pm}$  which compare the kinematic viscosity  $\nu$  to the thermal diffusivity  $\kappa$  and the magnetic diffusivity  $\eta = 1/(\mu\sigma)$ , respectively. Lastly, the aspect ratio  $\Gamma$  is the ratio of horizontal extend  $L$  of the fluid layer and the layer height  $H$ . The remaining quantities are the acceleration due to gravity  $g$ , the magnetic permeability  $\mu$ , the volumetric thermal expansion coefficient  $\alpha$  and the mass density  $\rho_0$  of the fluid at a reference temperature  $T_0$ . An alternative parameter to the Hartmann number is the Chandrasekhar number  $Q = \text{Ha}^2$ . Of major interest in the convection research are the globally averaged quantities of heat and momentum transport,

---

\* till.zuerner@ensta-paris.fr

	Reference	Pr	Ra <sub>min</sub>	Ra <sub>max</sub>	Ha <sub>min</sub>	Ha <sub>max</sub>	Γ
E	Cioni <i>et al.</i> [18]	0.025	$2 \times 10^7$	$3 \times 10^9$	850	1980	1 : 1
E	Aurnou and Olson [19]	0.025	$4 \times 10^2$	$7 \times 10^4$	26	35	8.3 : 8.3 : 1
E	Burr and Müller [20]	0.020	$3 \times 10^3$	$1 \times 10^5$	10	120	10 : 20 : 1
E	King and Aurnou [13]	0.024	$2 \times 10^6$	$2 \times 10^8$	0	1110	1 : 1
S	Liu <i>et al.</i> [22]	0.025	$1 \times 10^7$	$1 \times 10^7$	0	2000	4 : 4 : 1
S	Yan <i>et al.</i> [23]	1	$1 \times 10^4$	$8 \times 10^{10}$	0	10 000	periodic
		0.025	$2 \times 10^7$	$1.7 \times 10^8$	1414	1414	periodic
S	Lim <i>et al.</i> [24]	8	$5 \times 10^5$	$1 \times 10^{10}$	0	800	1 : 1 : 1
E	Zürner <i>et al.</i> [21]	0.029	$1 \times 10^6$	$6 \times 10^7$	0	1050	1 : 1
S	Akhmedagaev <i>et al.</i> [25]	0.025	$1 \times 10^7$	$1 \times 10^9$	0	1400	1 : 1

Table I. Parameters of available experimental and numerical data on RBC with a vertical magnetic field in chronological order. Listed are the Prandtl number Pr and the range of Rayleigh and Hartmann numbers (Ra<sub>min/max</sub> and Ha<sub>min/max</sub>). Experiments are marked by E and direct numerical simulations by S. In addition, the cell aspect ratio Γ is given as *diameter : height* for cylindrical cells and as *width : depth : height* for rectangular cells. For Cioni *et al.* [18], corresponding data at Ha = 0 were published in [10].

represented by the Nusselt and Reynolds number

$$\text{Nu} = 1 + \frac{H \langle u_z T \rangle}{\kappa \Delta T}, \quad \text{Re} = \frac{UH}{\nu}, \quad (2)$$

respectively. The symbol  $\langle \cdot \rangle$  denotes an average over the fluid volume and time. The characteristic velocity  $U$  is the speed of the mean wind in the convective flow. It is generally estimated by the root-mean-square (rms) average of the velocity field  $\mathbf{u}$  over the whole fluid volume  $U = \sqrt{\langle u_i^2 \rangle}$ . Another parameter of the magnetoconvection system is the magnetic Reynolds number  $\text{Rm} = \text{PmRe}$ . It compares the advection of the magnetic field by the flow to its diffusion. More detailed, at high  $\text{Rm} > 1$  the magnetic field can be deformed by the flow, while at low  $\text{Rm} \ll 1$  alterations to the external field  $\mathbf{B}_0$  can generally be neglected [1].

Experimental investigations of magnetoconvection require a working fluid with a sufficiently large electrical conductivity. In the vast majority of cases, liquid metals are the only option fitting this criterion. Their high electrical conductivity  $\sigma \sim 10^6$  S/m also gives them a good thermal conductivity which places them in the low Prandtl number regime  $\text{Pr} \ll 1$ . Experiments with a watery sulfuric acid ( $\text{Pr} = 12$ ,  $\sigma \sim 10^2$  S/m) do exist [8], though to reach the same Ha as in liquid metals magnetic fields of two orders of magnitude higher strength are required. Flow measurements in liquid metals are very difficult due to their opaque nature and high heat fluxes are necessary to reach large Rayleigh numbers compared to other common fluids such as air or water. Notable early works in liquid metal RBC without magnetic field include [9–12]. In recent years the topic experienced a number of new experimental efforts [13–17]. Experiments of RBC including the effects of a vertical magnetic field are much more rare. When the initial theory on heat and momentum transport [5] was published, only data by Cioni *et al.* [18] at high  $\text{Ha} \geq 850$  and Ra up to  $3 \times 10^9$  were available. Other studies were at very low  $\text{Ra} \leq 10^5$  and  $\text{Ha} \leq 120$  [19, 20]. Since then, experimental heat transport data by King and Aurnou [13] and Zürner *et al.* [21] were published, the latter including the currently sole measurements of the velocity field in liquid metal RBC with a vertical magnetic field. The parameter ranges covered by the now available experimental data are summarized in table I.

Numerical simulations of RBC with a vertical magnetic field at low Prandtl numbers are published by Liu *et al.* [22], Yan *et al.* [23] and Akhmedagaev *et al.* [25] (all at  $\text{Pr} = 0.025$ ). Simulations at higher Pr exist by Yan *et al.* [23] ( $\text{Pr} = 1$ ) and Lim *et al.* [24] ( $\text{Pr} = 8$ ). Their advantage over experiments is, of course, the full knowledge of the convective velocity field. However, for small Pr exhaustive parameter surveys are prohibitively expensive in terms of computation power. Nonetheless, their detailed insights on magnetoconvection are instrumental in revising the theoretical model. The parameters of the mentioned publications are also listed in table I.

This article is structured as follows. The next section II recapitulates the central ideas of the Grossmann-Lohse (GL) approach as the basis of the theoretical model. In section III the different parts of the magnetoconvection model are reviewed. Where necessary, they are altered or extended. The updated model is evaluated with the available experimental data and its results are discussed in section IV. Finally, section V gives the final conclusions and a short discussion.

## II. THE MAGNETOHYDRODYNAMIC EXTENSION OF THE GROSSMANN-LOHSE MODEL

For completeness, the framework of the theoretical model of heat and momentum transfer in magnetoconvection is outlined here. It is based on ref. [5] which builds on the original works by Grossmann and Lohse [6, 26–29], an updated parameter fit by Stevens *et al.* [30] (both for the nonmagnetic convection case, see also Bhattacharya *et al.* [31] for a slightly modified approach) and investigations by Chakraborty [7] for the magnetoconvection case. The GL theory considers the volume- and time-averaged viscous and thermal energy dissipation rates (DR) –  $\varepsilon_\nu$  and  $\varepsilon_\kappa$ , respectively – in the convective flow

$$\varepsilon_\nu = \frac{\nu}{2} \left\langle (\partial_i u_j + \partial_j u_i)^2 \right\rangle, \quad \varepsilon_\kappa = \kappa \left\langle (\partial_i T)^2 \right\rangle, \quad \varepsilon_\eta = \frac{\eta}{2} \left\langle (\partial_i b_j - \partial_j b_i)^2 \right\rangle. \quad (3)$$

Here, the Einstein summation convention is used over the coordinates  $i, j = x, y, z$  and  $\partial_i \equiv \partial/\partial x_i$  is a short notation for the spatial partial derivatives. In the case of magnetoconvection, the additional magnetic DR  $\varepsilon_\eta$  due to Joule dissipation has to be considered. Since the imposed magnetic field  $\mathbf{B}_0$  is homogeneous, only the secondary magnetic field  $\mathbf{b} = b_i \mathbf{e}_i$  induced by the interaction of  $\mathbf{u}$  and  $\mathbf{B}_0$  is relevant for the calculation of the magnetic DR. It should be mentioned that the above definition of  $\varepsilon_\eta$  differs by a factor of  $1/(\mu\rho_0)$  from other studies [5, 7]. This is done to have consistent units for the three dissipation rates:  $[\varepsilon_\nu] = (\text{m/s})^2/\text{s}$ ,  $[\varepsilon_\kappa] = \text{K}^2/\text{s}$  and  $[\varepsilon_\eta] = \text{T}^2/\text{s}$  with the above definitions. The GL approach is a mean field theory since only average quantities are considered. As a result, the aspect ratio  $\Gamma$  or the cell geometry is not incorporated explicitly into the theory and the effect of side walls, which can constrain the transport, is neglected. Only the top and bottom boundaries of the fluid layer are relevant. They are always assumed to be rigid and electrically insulating which results in a no-slip boundary condition for the velocity field.

The averaged DR in (3) are of importance since in statistically stationary turbulence the exact equations

$$\varepsilon_\nu + \frac{\varepsilon_\eta}{\mu\rho_0} = \frac{\nu^3}{H^4} \frac{(\text{Nu} - 1)\text{Ra}}{\text{Pr}^2}, \quad \varepsilon_\kappa = \kappa \frac{(\Delta T)^2}{H^2} \text{Nu} \quad (4)$$

can be obtained. In the original GL theory, the second term on the left-hand-side of the first equation is not present [6], since in that case  $\varepsilon_\eta = 0$ . The GL approach now splits the DR into their contributions from characteristic regions of the flow, namely the bulk and the boundary layer (BL)

$$\varepsilon_\nu = \varepsilon_{\nu,\text{Bulk}} + \varepsilon_{\nu,\text{BL}}, \quad \varepsilon_\eta = \varepsilon_{\eta,\text{Bulk}} + \varepsilon_{\eta,\text{BL}}, \quad \varepsilon_\kappa = \kappa \frac{(\Delta T)^2}{H^2} + \varepsilon_{\kappa,\text{Bulk}} + \varepsilon_{\kappa,\text{BL}}. \quad (5)$$

The term  $\kappa(\Delta T)^2/H^2$  for  $\varepsilon_\kappa$  is the contribution of pure heat conduction in the motionless base state of convection. For high Nusselt numbers this term is often neglected in comparison to the advection based contributions of the bulk and BL regions but becomes relevant in low-Nu regimes [29]. Now, the individual contributions in (5) are estimated by considering that the bulk dissipation is dominated by inertia and the BL dissipation by viscous effects. These estimates are then multiplied by free model parameters and combined with (4) and (5) to form the model equations. In the present article, the model fit parameters of the original GL theory are referred to by capital letters  $A$  and  $C_1$  to  $C_4$  (corresponding to  $a$  and  $c_1$  to  $c_4$  in [30]) and to the parameters of the present magnetoconvection model by small letters  $a$  and  $c_1$  to  $c_6$ . Note, that the parameters  $C_i$  and  $c_i$  do not correspond to the same terms. The reasoning for the initial estimates of the DR contributions in magnetoconvection can be found in [5]. They are listed here for completeness

$$\varepsilon_{\nu,\text{Bulk}} \sim \frac{U^3}{H} = \frac{\nu^3}{H^4} \text{Re}^3, \quad \varepsilon_{\nu,\text{BL}} \sim \nu \frac{U^2}{\delta_{v,B}^2} \frac{\delta_{v,B}}{H} = \frac{\nu^3}{H^4} \text{Re}^2 \text{Ha}, \quad (6a)$$

$$\varepsilon_{\eta,\text{Bulk}} \sim \eta \frac{\text{Rm}^2 B_0^2}{H^2} = \mu\rho_0 \frac{\nu^3}{H^4} \text{Re}^2 \text{Ha}^2, \quad \varepsilon_{\eta,\text{BL}} \sim \eta \frac{\text{Rm}^2 B_0^2}{\delta_{v,B}^2} \frac{\delta_{v,B}}{H} = \mu\rho_0 \frac{\nu^3}{H^4} \text{Re}^2 \text{Ha}^3, \quad (6b)$$

$$\varepsilon_{\kappa,\text{Bulk}} \sim \frac{(\Delta T)^2 U}{H} = \kappa \frac{(\Delta T)^2}{H^2} \text{RePr}, \quad \varepsilon_{\kappa,\text{BL}} \sim \kappa \frac{(\Delta T)^2}{H^2} \sqrt{\text{RePr}}. \quad (6c)$$

The above estimates are based on the following assumptions: (i) The Prandtl number is restricted to the  $\text{Pr} \ll 1$  case of liquid metals. (ii) The Hartmann number is high enough, that the viscous boundary layers at the top and bottom boundary have to be substituted by Hartmann layers. The viscous BL thickness  $\delta_v$  transforms then to  $\delta_{v,B} = H/\text{Ha}$ . Recall that the original GL theory assumed a Blasius-type BL with a thickness  $\delta_{v,0} = aH/\sqrt{\text{Re}}$ , where  $a$  is a free parameter [26]. The thermal BL thickness given by  $\delta_T = H/(2\text{Nu})$  is unaffected by this assumption [25]. (iii) The

magnetic Reynolds number is sufficiently low,  $\text{Rm} \ll 1$ , so that the quasistatic approximation can be applied. Then the effect of the induced magnetic field  $\mathbf{b}$  on the eddy currents can be neglected compared to the external magnetic field  $\mathbf{B}_0$ . Since liquid metals have  $\text{Pm} \sim 10^{-6}$ , very high Reynolds numbers of  $\text{Re} \sim 10^6$  are needed to invalidate this assumption. In this approximation, the magnitude of  $\mathbf{b}$  can be estimated as  $b \sim \text{Rm}B_0$ .

Additionally, three regime transitions are introduced to account for changes in the estimates (6) for different parameter regimes. First, the velocity scale within the thermal BL is  $U$  if  $\delta_T > \delta_v$ . However for the case  $\delta_T < \delta_v$ , the velocity scale becomes  $U\delta_T/\delta_v$  [6]. This change in scaling is introduced by replacing  $\text{Re} \rightarrow \text{Re}f(\delta_{v,B}/\delta_T)$  in (6c) with the transition function  $f(x) = (1+x^n)^{-1/n}$ , where  $n = 4$  [26]. Secondly,  $\varepsilon_{\nu,\text{Bulk}} \propto \text{Re}^3$  in (6a) assumes a turbulent flow, while after a transition to a weakly non-linear flow the scaling is better represented by  $\varepsilon_{\nu,\text{Bulk}} \propto \text{Re}^2$ . This is facilitated by multiplying  $\varepsilon_{\nu,\text{Bulk}}$  by  $g(\text{Re}/\text{Re}^*)$ , where  $g(x) = f(1/x)^{-1}$  and  $\text{Re}^*$  is a model parameter characterizing the position of transition to fully turbulent convection [5]. The last transition concerns the onset of convection, which is not naturally recovered by the model and is imposed by replacing occurrences of  $\text{Nu} - 1$  by  $(\text{Nu} - 1)/h(\text{Ra}/\text{Ra}_c)$  with the transition function  $h(x) = 1 - f(x)$ . The critical Rayleigh number  $\text{Ra}_c$  is calculated in the Chandrasekhar limit  $\text{Ra}_c = \pi^2\text{Ha}^2$  [32] which is valid for  $\text{Ha} \gtrsim 100$ . This last replacement has to be done only in the model equation used to calculate  $\text{Nu}$  [5].

With these considerations implemented, the final model equations are calculated by multiplying the estimates (6) with free model parameters  $c_1$  to  $c_6$  and combining them with (4) and (5). The result is [5]

$$\text{Re} = \frac{\left(\sqrt{c_6^2 + 4c_5(\text{Nu} - 1)} - c_6\right)^2}{4c_3^2\text{Pr}f\left(\frac{2\text{Nu}}{\text{Ha}}\right)}, \quad (7a)$$

$$\frac{(\text{Nu} - 1)\text{Ra}}{\mathcal{R}^2\text{Pr}^2h(\text{Ra}/\text{Ra}_c)} = c_1\mathcal{R}g\left(\frac{\mathcal{R}}{\text{Re}^*}\right) + c_2\text{Ha} + c_3\text{Ha}^2 + c_4\text{Ha}^3 \quad \text{with } \mathcal{R} = \frac{\left(\sqrt{c_6^2 + \frac{4c_5(\text{Nu}-1)}{h(\text{Ra}/\text{Ra}_c)}} - c_6\right)^2}{4c_5^2\text{Pr}f\left(\frac{2\text{Nu}}{\text{Ha}}\right)}. \quad (7b)$$

Equation (7b) contains  $\text{Nu}$ ,  $\text{Ra}$ ,  $\text{Ha}$  and  $\text{Pr}$  only. If the values of the model parameters  $c_1$  to  $c_6$  and  $\text{Re}^*$  are known, it can be used to numerically calculate  $\text{Nu}$  for a point in the  $(\text{Ra}, \text{Ha}, \text{Pr})$  parameter space. Once  $\text{Nu}$  is known,  $\text{Re}$  can be obtained from (7a).

Since the model parameters  $c_1$  to  $c_6$  and  $\text{Re}^*$  are *a priori* unknown, they have to be determined by fitting equations (7) to experimental data sets of  $(\text{Ra}, \text{Ha}, \text{Pr}, \text{Nu})$  and at least one data point  $(\text{Ra}, \text{Ha}, \text{Pr}, \text{Nu}, \text{Re})$  including the Reynolds number. In [5], using the heat transfer data by Cioni *et al.* [18] and numerical results for the momentum transport, the parameter values  $c_1 = 0.053$ ,  $c_2 = -2.4$ ,  $c_3 = 0.014$ ,  $c_4 = -3.7 \times 10^{-6}$ ,  $c_5 = 0.0038$ ,  $c_6 = 0.47$  and  $\text{Re}^* = 5.6 \times 10^4$  were obtained. Figure 1 shows the regime diagrams of the GL theory at  $\text{Ha} = 0$  [30] and of the initial model at  $\text{Pr} = 0.025$  [5]. These will be used as reference in the following discussion.

### III. MODIFICATIONS OF THE FRAMEWORK

The original model can be significantly revised by considering the validity boundaries of the model and which assumptions or mechanisms are applicable in that range of parameters. Each of the following sections considers one aspect of the initial model equations (7). Some aspects of the previous model will be corrected as required and new aspects are introduced.

#### A. Crossover of the thermal and kinetic BL

The first topic concerns the velocity scale within the thermal BL. As discussed in section II, the characteristic velocity is chosen as  $U$  if  $\delta_T > \delta_v$  and as  $(\delta_T/\delta_v)U$  if  $\delta_T < \delta_v$ , which is implemented by the transition function  $f(\delta_{v,B}/\delta_T)$  in the initial model (7) and by  $f(\delta_{v,0}/\delta_T)$  in the GL theory [26]. This, however, entails an unnecessary complication of the model for low  $\text{Pr}$ . Simulations [33, 34] at  $\text{Ha} = 0$  and  $\text{Pr} = 0.025$  show that the viscous BL is smaller than the thermal BL  $\delta_v < \delta_T$ . This is also reflected by the results of the GL theory which gives the BL crossover  $\delta_{v,0} = \delta_T$  for  $\text{Pr} > 0.1$  up to  $\text{Ra} = 10^{11}$  (figure 1(a)). By applying a magnetic field, the kinetic BL is decreased due to its eventual transformation into a Hartmann layer  $\delta_{v,B} \propto 1/\text{Ha}$  [24]. Conversely, the thermal boundary layer thickness  $\delta_T \propto 1/\text{Nu}$  increases since experiments and simulations in low- $\text{Pr}$  magnetoconvection have shown that  $\text{Nu}$  generally decrease for increasing  $\text{Ha}$  [13, 18, 21, 22]. That means that the presence of the  $\delta_{v,B} = \delta_T$  regime boundary in the initial model (see dashed line in figure 1(b)) is implausible and a result of the insufficient coverage of the low- $\text{Ha}$  regime by the experimental data used for fitting the model parameters. The discrepancy between the model and experimental data is shown in figure 2. Measured Nusselt numbers taken from Zürner *et al.*

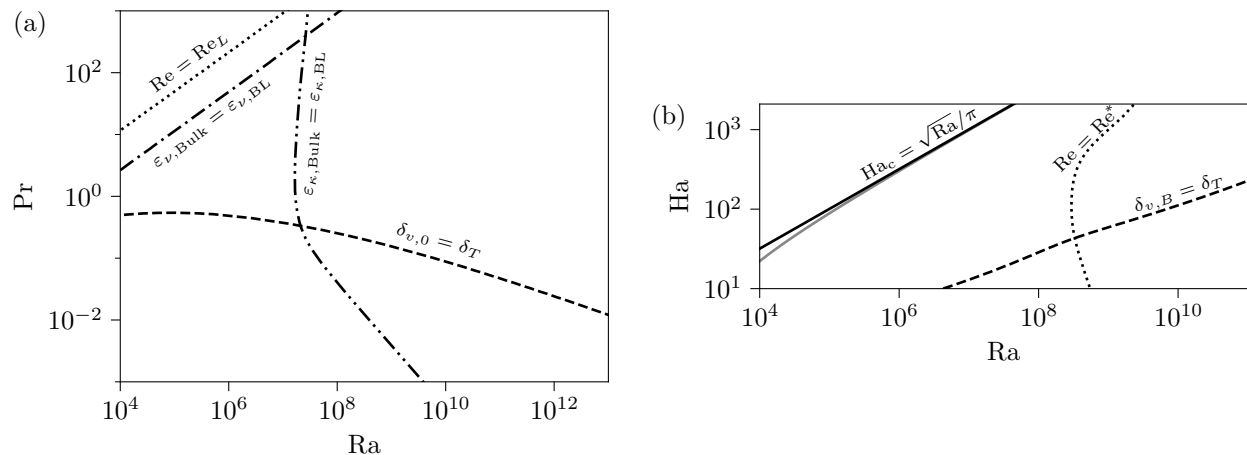


Figure 1. (a) Phase diagram of the GL theory at  $Ha = 0$  spanned by Rayleigh number  $Ra$  and Prandtl number  $Pr$  according to Stevens *et al.* [30]. Shown are the transition boundaries for the BL crossover  $\delta_{v,0} = \delta_T$  (dashed line), the equivalence of bulk and BL dissipation for the viscous DR  $\varepsilon_{\nu,Bulk} = \varepsilon_{\nu,BL}$  (dash-dotted line) and thermal DR  $\varepsilon_{\kappa,Bulk} = \varepsilon_{\kappa,BL}$  (dash-double-dotted line) and the transition to the large- $Pr$  regime at  $Re = Re_L = 3.4$  (dotted line). (b)  $(Ra, Ha)$  phase diagram of the initial model for magnetoconvection at  $Pr = 0.025$  according to Zürner *et al.* [5]. Shown are the transition boundaries for the BL crossover  $\delta_{v,B} = \delta_T$  (dashed line), the transition to the fully turbulent regime at  $Re = Re^* = 5.6 \times 10^4$  (dotted line) and the Chandrasekhar limit  $Ha_c = \sqrt{Ra}/\pi$  (solid line). For comparison, the real solution of  $Ha_c$  from a linear stability analysis [32] is plotted as a gray solid line.

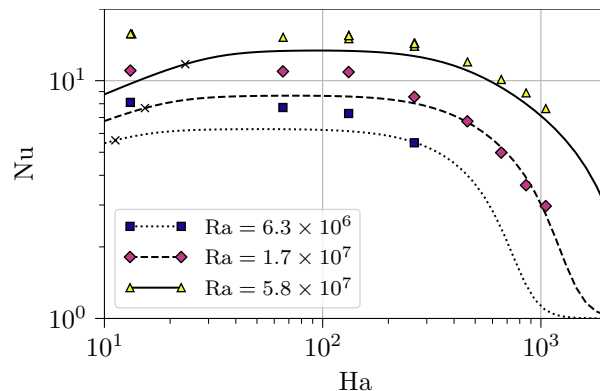


Figure 2. Comparison of experimental Nusselt number data (symbols) from [21] with the predictions of the initial model (7) (lines) at  $Pr = 0.029$  for selected  $Ra$ . The position of the BL crossover  $\delta_{v,B} = \delta_T$  is marked by crosses on the respective lines.

[21] (symbols) are compared to the predictions of the initial model (7) (lines) at three selected  $Ra$ . For high  $Ha > 200$ , the model captures the experimental results well, but deviates from the experiments at small  $Ha$ . Especially for  $Ha \rightarrow 0$ , the experimental  $Nu$  data saturate at a constant value while the model predictions start to decrease. This coincides with the boundary layer crossover  $\delta_{v,B} = \delta_T$  which is marked by a cross on each line. These considerations show that the BL crossover is not relevant for small  $Pr$  and can actually result in wrong predictions for the low- $Ha$  regime. It will thus be eliminated from the revised model equations, i.e., the transition function  $f$  is removed.

The BL crossover only becomes relevant at moderate or high  $Pr$ . Simulations of magnetoconvection at  $Pr = 8$  [24] found a BL crossover with  $\delta_v > \delta_T$  below an optimal Hartmann number. It is also of interest that the crossover is tied to a short increase of the Nusselt number compared to its value at  $Ha = 0$ . As seen in figure 2, the transition function  $f$  emulates such a behavior by generating a local maximum of  $Nu$ . That means, if the present model was to be extended to the intermediate and high  $Pr$  case the transition function  $f$  may be of importance and could be reintroduced. However, this is not part of the scope of the present work.

## B. The limit of small Hartmann numbers

In the model equations (7), the Hartmann BL  $\delta_{v,B} = H/\text{Ha}$  is used to characterize the kinetic BL. This is not applicable for the limit  $\text{Ha} \rightarrow 0$ , where the kinetic BL is better described by a Prandtl-Blasius type BL  $\delta_{v,0} = aH/\sqrt{\text{Re}}$  as used by the GL theory [6]. Lim *et al.* [24] proposed a general BL thickness  $\delta_v$  based on a dimensional analysis that connects these two types of BL

$$\delta_v = \left( \delta_{v,0}^{-2} + \delta_{v,B}^{-2} \right)^{-1/2} = \frac{H}{\sqrt{\text{Re}/a^2 + \text{Ha}^2}}. \quad (8)$$

For high  $\text{Ha} \rightarrow \infty$ , (8) becomes a Hartmann layer  $\delta_v \rightarrow \delta_{v,B}$  and at vanishing magnetic fields the Prandtl-Blasius BL is recovered  $\delta_v \rightarrow \delta_{v,0}$ . Replacing  $\delta_{v,B}$  with  $\delta_v$  in the BL contribution of the kinetic and magnetic DR in (6a) and (6b) results in the modified estimates

$$\varepsilon_{\nu,\text{BL}} \sim \nu \frac{U^2}{\delta_v^2} \frac{\delta_v}{H} = \frac{\nu^3}{H^4} \sqrt{\text{Re}^5/a^2 + \text{Re}^4 \text{Ha}^2}, \quad (9a)$$

$$\varepsilon_{\eta,\text{BL}} \sim \eta \frac{\text{Rm}^2 B_0^2}{\delta_v^2} \frac{\delta_v}{H} = \mu \rho_0 \frac{\nu^3}{H^4} \sqrt{\text{Re}^5 \text{Ha}^4/a^2 + \text{Re}^4 \text{Ha}^6}. \quad (9b)$$

In the high  $\text{Ha}$  limit, these estimates recover the initial scalings (6). For  $\text{Ha} \rightarrow 0$ ,  $\varepsilon_{\eta,\text{BL}}$  vanishes and  $\varepsilon_{\nu,\text{BL}}$  becomes the estimate of the original GL theory  $\varepsilon_{\nu,\text{BL}} \sim (\nu^3/H^4)\text{Re}^{5/2}$  [6].

## C. Transition towards laminar bulk flow and onset of convection

The original GL ansatz [6] assumes the existence of a turbulent large-scale wind of velocity  $U$  in the convection cell. Even with the subsequent extension towards a laminar high-Pr case [26], the scaling of the viscous bulk DR has always been assumed to be dominated by inertia ( $\varepsilon_{\nu,\text{Bulk}} \propto \text{Re}^3$ ). The initial model for magnetoconvection [5] introduced a transition between the turbulent  $\text{Re}^3$ -scaling towards a laminar  $\text{Re}^2$ -scaling of  $\varepsilon_{\nu,\text{Bulk}}$  at a characteristic Reynolds number of  $\text{Re}^*$  which was evaluated to  $\text{Re}^* = 5.6 \times 10^4$ . The phase diagram in figure 1(b) shows this transition to happen at  $\text{Ra} > 10^8$  for all  $\text{Ha}$ . However, especially for the  $\text{Ha} = 0$  case it is well-known that turbulence in low-Pr convection sets in at much smaller  $\text{Ra}$  [35–37]. Since the bulk turbulence is a central assumption of the model, it is evident that this scaling transition on its own is insufficient to model the weakly non-linear and laminar regimes at high  $\text{Ha}$ . The transition function  $g$  and the model parameter  $\text{Re}^*$  are consequently removed from the model equations.

The onset of convection cannot be recovered intrinsically by the current model and would require a proper treatment of the non-turbulent regimes with a complete overhaul of the model ansatz. This, however, is beyond the scope of this study. The transition towards the purely conductive regime was previously imposed at the Chandrasekhar limit by a fixed transition function  $h$  in [5]. This approach will be retained and the results of the revised model with and without the imposed onset transition are compared in section IV.

The critical Rayleigh number in the Chandrasekhar limit  $\text{Ra}_c = \pi^2 \text{Ha}^2$  is valid only for  $\text{Ha} \gtrsim 100$ . To allow for the limit  $\text{Ha} \rightarrow 0$  discussed in the previous section, the argument of the onset transition function  $h$  is replaced based on the critical Hartmann number:  $h(\text{Ha}_c^2/\text{Ha}^2)$ . In the Chandrasekhar limit,  $\text{Ha}_c = \sqrt{\text{Ra}}/\pi$  which is valid for  $\text{Ra} \gtrsim 2 \times 10^5$  and all  $\text{Ha}$  with a deviation of  $\leq 10\%$  from the proper solution obtained by a linear stability analysis [32]. Since  $\text{Ha}_c^2/\text{Ha}^2 = \text{Ra}/\text{Ra}_c$  in the Chandrasekhar limit, this change has only an effect on the validity boundaries of the model.

Recently, simulations [22] and experiments [21] proved the existence of convective flows for  $\text{Ha} > \text{Ha}_c$  concentrated near the lateral walls of the convection cell. They are denoted as wall modes that cannot be included in the present mean-field theory which neglects the effect of side-walls.

## D. Revised model equations

The initial and new DR contribution estimates (6) and (9) are multiplied by the model parameters  $c_1$  to  $c_6$  and combined with equations (4) and (5)

$$\frac{(\text{Nu} - 1)\text{Ra}}{\text{Pr}^2} = c_1\text{Re}^3 + c_2\sqrt{\text{Re}^5/a^2 + \text{Re}^4\text{Ha}^2} + c_3\text{Re}^2\text{Ha}^2 + c_4\sqrt{\text{Re}^5\text{Ha}^4/a^2 + \text{Re}^4\text{Ha}^6}, \quad (10)$$

$$\text{Nu} - 1 = c_5\text{RePr} + c_6\sqrt{\text{RePr}}. \quad (11)$$

For the case  $\text{Ha} = 0$ , the second model equation (11) does not change while equation (10) becomes

$$\frac{(\text{Nu} - 1)\text{Ra}}{\text{Pr}^2} = c_1\text{Re}^3 + \frac{c_2}{a}\text{Re}^{5/2}. \quad (12)$$

(12) and (11) are equal to the GL model equations [30] for the low-Pr regime, i.e., if the regime transitions for the BL crossing and for the high-Pr limit are removed. Consequently, the parameters in (12) and (11) can be identified with the values of the GL theory

$$a = A = 0.922, \quad c_1 = C_2 = 1.38, \quad c_2 = AC_1 = 7.42, \quad c_5 = C_4 = 0.0252, \quad c_6 = C_3 = 0.487, \quad (13)$$

with  $C_1 = 8.05$  [30]. The only remaining unknown parameters are thus  $c_3$  and  $c_4$ . This is a significant reduction of the number of free parameters compared to the seven fit coefficients of the initial model. The two remaining parameters need to be fitted to experimental data. The original fit [5] resulted in some negative parameter values. Since only positive coefficients are physically sensible for dissipation rates, the bounds  $(0, \infty)$  are imposed on the two parameters during the fitting process.

The initial model for magnetoconvection as well as the GL theory suffer from a certain ambiguity of the parameters regarding the absolute value of the Reynolds number and required at least one full set of data ( $\text{Ra}, \text{Ha}, \text{Pr}, \text{Nu}, \text{Re}$ ) to resolve this issue (see also the appendix for details). Due to the choice (13) of the parameters  $a, c_1, c_2, c_5$  and  $c_6$ , this ambiguity has already been fixed for the present model and does not require further consideration.

To fit the model equations to data sets of  $(\text{Ra}, \text{Ha}, \text{Pr}, \text{Nu})$ , the Reynolds number is eliminated from (10) using (11). To impose the onset of convection,  $\text{Nu} - 1$  is replaced by  $(\text{Nu} - 1)/h(\text{Ha}_c^2/\text{Ha}^2)$ , where  $h(x) = 1 - (1 + x^4)^{-1/4}$  [5]

$$\begin{aligned} \frac{(\text{Nu} - 1)\text{Ra}}{h(\text{Ha}_c^2/\text{Ha}^2)\text{Pr}^2} &= C_2\mathcal{R}^3 + AC_1\sqrt{\mathcal{R}^5/A^2 + \mathcal{R}^4\text{Ha}^2} + c_3\mathcal{R}^2\text{Ha}^2 + c_4\sqrt{\mathcal{R}^5\text{Ha}^4/A^2 + \mathcal{R}^4\text{Ha}^6}, \\ \mathcal{R} &= \frac{\left(\sqrt{C_3^2 + 4C_4(\text{Nu} - 1)/h(\text{Ha}_c^2/\text{Ha}^2)} - C_3\right)^2}{4C_4^2\text{Pr}}. \end{aligned} \quad (14)$$

Once the values of  $c_3$  and  $c_4$  are determined, (14) can be numerically solved for  $\text{Nu}$  with a given set of  $(\text{Ra}, \text{Ha}, \text{Pr})$ . The corresponding value of  $\text{Re}$  then follows from (11) to

$$\text{Re} = \frac{\left(\sqrt{C_3^2 + 4C_4(\text{Nu} - 1)} - C_3\right)^2}{4C_4^2\text{Pr}}. \quad (15)$$

#### IV. RESULTS

The model equation (14) is fitted to the experimental data sets  $(\text{Ra}, \text{Ha}, \text{Pr}, \text{Nu})$  by Cioni *et al.* [18], King and Aurnou [13] and Zürner *et al.* [17]. The resulting parameter values of the model including the onset of convection are

$$c_3 = 0.0449, \quad c_4 = 7.52 \times 10^{-18} \approx 0. \quad (16)$$

The  $c_4$ -term vanishes, i.e.,  $\varepsilon_{\eta, \text{BL}}$  has no influence on the result. This means either that the effect of Joule dissipation in the viscous BL is negligible or that it is only relevant at high magnetic fields  $\text{Ha} > 2000$ , beyond the currently available experiments (see table I). The latter could be the case, since  $\varepsilon_{\eta, \text{BL}} \propto \text{Ha}^3$  may increase significantly for high  $\text{Ha}$ . If the onset of convection is excluded (i.e.,  $h(x) = 1$ ), the fitted parameter values become  $c_3 = 0.0520$  and  $c_4 = 5.19 \times 10^{-19}$  which shows no significant difference to (16). Lifting the fitting boundaries of  $(0, \infty)$  results in a small negative value of  $c_4 \sim -10^{-5}$  which does not affect the results of the equations significantly. It can, however, cause unstable numerical solutions of the model equations for  $\text{Ha} \gtrsim 1000$ . This reinforces the choice of the restriction of  $c_3$  and  $c_4$  to positive values and that  $c_4$  vanishes.

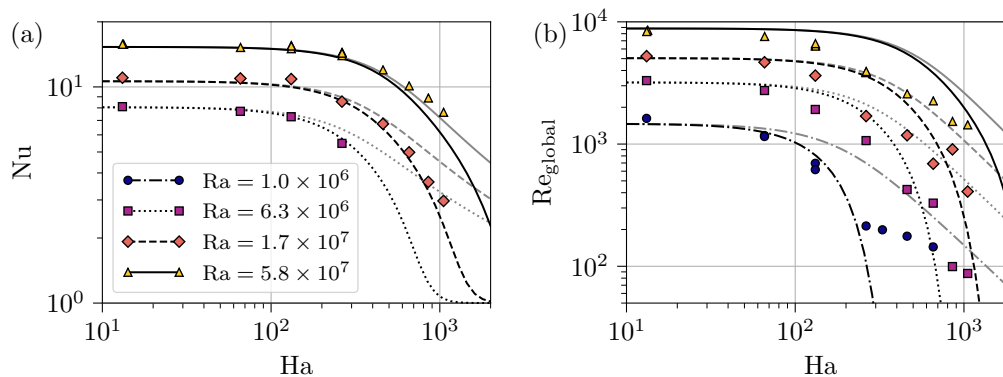


Figure 3. Comparison of results from the theoretical model (lines) with experimental data by Zürner *et al.* [21] (markers). Values of (a) Nu and (b)  $Re_{\text{global}}$  are plotted vs. Ha for selected Ra.  $Re_{\text{global}}$  is based on the rms-average of all velocity data measured in the experiments. Black (gray) lines correspond to the model with (without) imposed onset of convection.

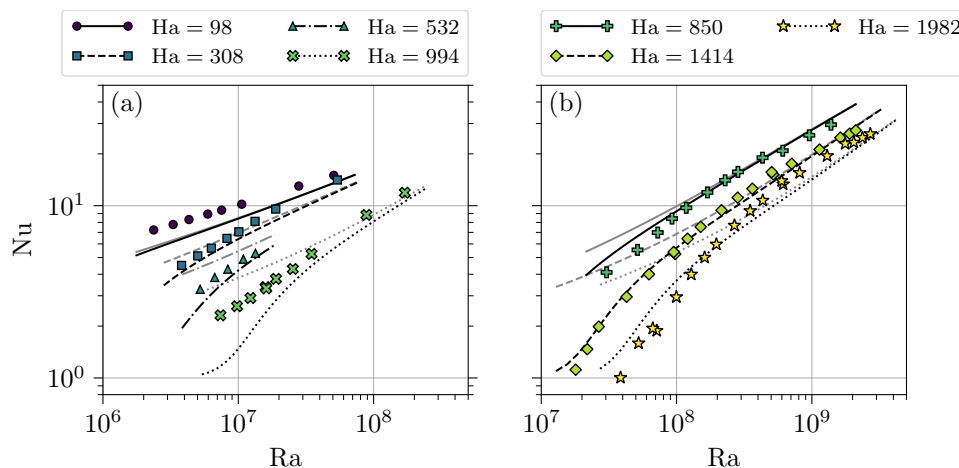


Figure 4. Comparison of results from the theoretical model (lines) with experimental data from (a) King and Aurnou [13] and (b) Cioni *et al.* [18] (markers). Nu is plotted vs. Ra for selected Ha. Black (gray) lines correspond to the model with (without) imposed onset of convection.

### A. Comparison with experimental data

Figures 3(a) and 4 compare the Nusselt number calculated from the model equation (14) with the experimental data used for fitting the parameters  $c_3$  and  $c_4$ . First, the model including the onset of convection is discussed (black lines). The data by Zürner *et al.* [21] in figure 3(a) are well reproduced by the model. Especially for  $Ha \rightarrow 0$ , the model fits much better than the initial model (see figure 2). Only close to the onset of convection does the model underpredict the experimental data slightly. Nusselt number data by Cioni *et al.* [18] (figure 4(b)) also fit well with the theoretical results. Here, the model generally overpredicts the experimental data near the onset of convection. The exact progression of Nu with increasing Ra is not exactly the same, with the model approaching a straight line (i.e., a power law) while the experiment showing a curvature, but the general trend and order of magnitude is recovered. The data by King and Aurnou [13] fits less well with the model (figure 4(a)). The model approaches the data with increasing Ra, but consistently underpredicts the experiment. Especially for  $Ha = 994$ , the onset of convection at the Chandrasekhar limit is not visible in the experiment. This is in stark contrast to the other experiments (e.g. the  $Ha = 850$  data in figure 4(b)). In light of this discrepancy between the experimental data, the model manages to create a satisfactory reproduction of the Nusselt number.

The model without onset of convection (gray lines) is identical to the previous case for low Ha and high Ra but deviates strongly close to the Chandrasekhar limit. This shows that the model is not intrinsically applicable outside of turbulent convection and why Chandrasekhar limit is imposed explicitly using a transition function.

Experimental Re data are available from the experiments by Zürner *et al.* [21]. The velocity field is probed using ten ultrasound Doppler velocimetry (UDV) sensors and a characteristic global velocity scale is calculated as a rms-

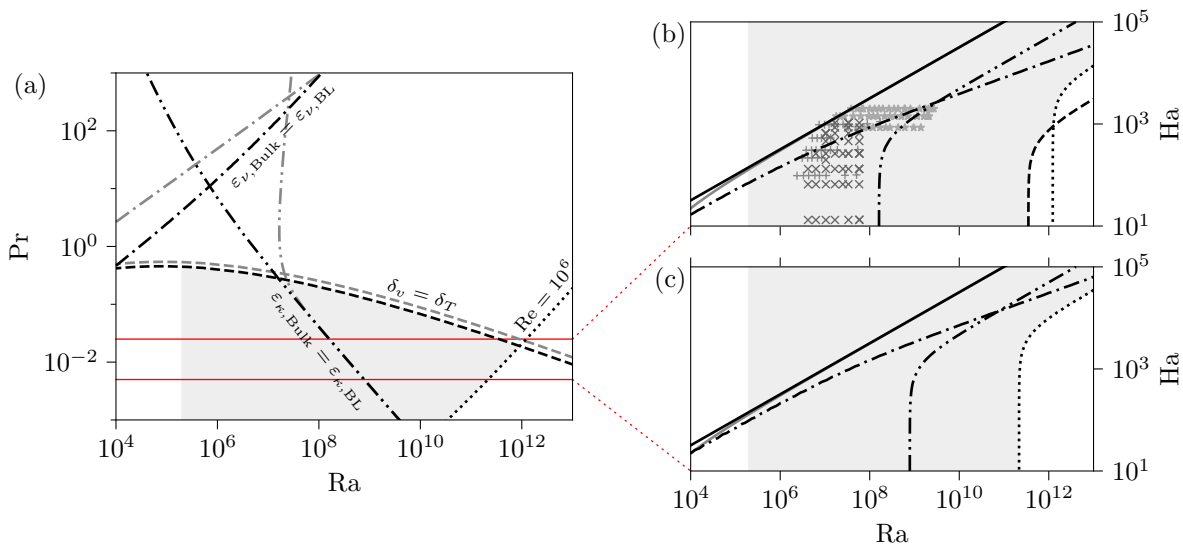


Figure 5. Regime diagram and validity boundaries (gray shaded areas) of the revised magnetoconvection model including the onset of convection. (a)  $(Ra, Pr)$  phase diagram for  $Ha = 0$ . Shown are the transition boundaries for the BL crossover  $\delta_v = \delta_T$  (dashed line),  $Re = 10^6$  (dotted line) and the equivalence of bulk and BL dissipation for the viscous DR  $\varepsilon_{\nu, \text{Bulk}} = \varepsilon_{\nu, \text{BL}}$  (dash-dotted line) and thermal DR  $\varepsilon_{\kappa, \text{Bulk}} = \varepsilon_{\kappa, \text{BL}}$  (dash-double-dotted line). The corresponding regime boundaries of the GL theory [30] are re-plotted as gray lines from figure 1(a). (b) and (c)  $(Ra, Ha)$  phase diagram for  $Pr = 0.025$  (mercury, gallium) and  $Pr = 0.005$  (sodium), respectively. These Prandtl numbers are marked in (a) by horizontal lines. The critical Hartmann number  $Ha_c$  is displayed in the Chandrasekhar limit (solid black line) and as the rigorous linear stability solution (gray solid line). The remaining lines correspond to the regime boundaries in (a). The gray markers in (b) indicate the experiments used to fit the revised model: Cioni *et al.* [18] (stars), King and Aurnou [13] (pluses) and Zürner *et al.* [21] (crosses).

average over time and over all sensors. The resulting global Reynolds number  $Re_{\text{global}}$  is compared to the model in figure 3(b). In the low- $Ha$  limit, the model and  $Re_{\text{global}}$  have the same values, though this should be interpreted as purely coincidental. As shown in [17], the GL theory underpredicts Reynolds numbers based on the turbulent large-scale wind in low- $Pr$  convection by nearly a factor of two. At the same time, the magnitude of  $Re_{\text{global}}$  is affected by many low-velocity areas of the flow and coincidentally is also about half the magnitude of a wind-based Reynolds number [21]. It is possible to re-scale the theoretical Reynolds number to match the wind-based Reynolds number from experiments, the effects of which are shown in the appendix.

As can be seen in figure 3, the Reynolds number starts to decrease from its value at  $Ha = 0$  at lower  $Ha$  than the Nusselt number [21]. Since in equation (15)  $Re$  is directly linked to  $Nu$ , the model does not recover this behavior and  $Re$  stays constant up to the value of  $Ha$  where  $Nu$  starts to drop off. Also, the onset transition function forces  $Re$  to drop off very fast while  $Re_{\text{global}}$  decreases much slower due to the presence of wall modes past the Chandrasekhar limit. The main issue is that in magnetoconvection, the degree of turbulence in the flow is not directly linked to the magnitude of the Reynolds number of the average velocity magnitude. A combination of high  $Ra$  and high  $Ha$  might produce the same Reynolds number of the large scale flow as another combination of low  $Ra$  and low  $Ha$ , but with weaker turbulent fluctuations [21]. This disconnects the progression of  $Re$  from the progression of  $Nu$ , the latter being dependent on the mean velocity magnitude as well as velocity fluctuations [24]. This effect is not included in the model equations and as a result, the model is not recovering the progression of the Reynolds number correctly, except for the low- $Ha$  limit.

## B. Regime diagram and validity boundaries

Figure 5(a) shows the phase diagram of the revised model at  $Ha = 0$  (black lines) in comparison to the GL theory (gray lines). The BL crossover ( $\delta_v = \delta_T$ , dashed line) is positioned at only slightly smaller  $Pr$  than the result of the GL theory. Below this line ( $\delta_v < \delta_T$ ), the regime boundaries of the thermal DR contribution crossover ( $\varepsilon_{\kappa, \text{Bulk}} = \varepsilon_{\kappa, \text{BL}}$ , dash-double-dotted line) coincide for the revised model and the GL theory. This is expected since the model recovers the GL model equations in the low- $Pr$  limit. For  $Pr$  above the BL crossover ( $\delta_v > \delta_T$ ), these regime boundaries and the kinetic DR contribution crossover ( $\varepsilon_{\nu, \text{Bulk}} = \varepsilon_{\nu, \text{BL}}$ , dash-dotted line) deviate strongly from one another, indicating that the model is not applicable for these regimes.

The validity of the model is limited by the following assumptions. (i) The working fluid has a low Prandtl number  $\text{Pr} \ll 1$ . This implies that  $\delta_v < \delta_T$  and the BL crossover is thus considered as regime boundary for the low-Pr regime. (ii) The Chandrasekhar limit is assumed for the critical Hartmann number  $\text{Ha}_c = \sqrt{\text{Ra}}/\pi$  which is valid for  $\text{Ra} > 2 \times 10^5$ . (iii) The quasistatic approximation applies, i.e.,  $\text{Rm} \ll 1$ . For a typical magnetic Prandtl number for liquid metals of  $\text{Pm} \sim 10^{-6}$ , this implies that a Reynolds number of  $\text{Re} \sim 10^6$  has to be reached to violate this assumption. The gray shaded area in figure 5(a) shows the validity range of the revised model defined by the above boundaries (i) to (iii). For decreasing and increasing  $\text{Ra}$ , the limiting boundaries are  $\text{Ra} = 2 \times 10^5$  and  $\text{Re} = 10^6$  (dotted line), respectively. With increasing  $\text{Pr}$ , the model reaches up to the  $\delta_v = \delta_T$  boundary (dashed line).

Turning to the case  $\text{Ha} > 0$ , figures 5(b) and (c) show the  $(\text{Ra}, \text{Ha})$  phase diagrams for the characteristic Prandtl numbers  $\text{Pr} = 0.025$  (mercury, gallium) and  $\text{Pr} = 0.005$  (sodium), respectively. Displayed are the same regime boundaries as in figure 5(a) together with the Chandrasekhar limit (solid black line). Since the revised model is applicable for all Hartmann numbers, there are no vertical boundaries to the validity range (gray shaded areas). For low  $\text{Ra}$ , the model is, again, limited by  $\text{Ra} = 2 \times 10^5$ . For high  $\text{Ra}$  and  $\text{Pr} = 0.025$ , the validity boundaries are the BL crossover at low  $\text{Ha} \lesssim 10^3$  and the  $\text{Re} = 10^6$  boundary for higher  $\text{Ha}$ . At  $\text{Pr} = 0.005$ , the BL crossover is shifted to very high  $\text{Ra} > 10^{14}$  (see also figure 5(a)) and the  $\text{Re} = 10^6$  boundary is the limiting restriction when increasing  $\text{Ra}$  for all  $\text{Ha}$ . Since the validity of the quasistatic approximation is dependent on the magnetic Prandtl number, these limits may shift for increasing or decreasing  $\text{Pm}$  (the boundary is shifted to smaller or higher  $\text{Ra}$ , respectively).

The DR contribution crossovers for the kinetic and thermal DR are also plotted in figures 5(b) and (c) (dash-dotted and dash-double-dotted lines, respectively).  $\varepsilon_{\nu, \text{Bulk}}$  is dominant at low  $\text{Ha}$  but is eventually surpassed by  $\varepsilon_{\nu, \text{BL}}$  when  $\text{Ha}$  increases. The thermal DR is generally more dependent on  $\text{Ra}$  with  $\varepsilon_{\kappa, \text{BL}}$  and  $\varepsilon_{\kappa, \text{Bulk}}$  being dominant at low and high  $\text{Ra}$ , respectively. With decreasing  $\text{Pr}$ , the kinetic DR crossovers is shifted to higher  $\text{Ha}$ . The thermal DR crossover at low  $\text{Ha}$  shifts to higher  $\text{Ra}$  for decreasing  $\text{Pr}$ . At high  $\text{Ha}$ , however, it is unaffected by changes in  $\text{Pr}$  and runs parallel to the Chandrasekhar limit. Since the parameter  $c_4$  is extremely small, the magnetic DR is dominated by  $\varepsilon_{\eta, \text{Bulk}}$  for all  $\text{Ra}$  and  $\text{Ha}$ .

In summary, the comparison with experimental data (figures 3 and 4) and the phase diagrams (figure 5) show that despite the reduced complexity of the revised model, its predictions are more accurate and more physically sensible compared to the previous model [5].

## V. CONCLUSION

An updated model of the heat and momentum transport for Rayleigh-Bénard convection in a vertical magnetic field was presented. By revising some of the basic assumptions of the model and including new aspects, the theoretical predictions could be improved significantly. The inclusion of a generalized kinetic boundary layer thickness allowed for the extension of the model to the low- $\text{Ha}$  limit and to match it with the well established Grossmann-Lohse theory at  $\text{Ha} = 0$ . This reduced the complexity of the model significantly by fixing the values of five parameters. With the removal of the turbulent-to-laminar transition, the total number of free model parameters has thus been reduced from the initial seven to just two. An extended experimental database also allowed for a more robust fit of the model which effectively removed one more parameter ( $c_4 \approx 0$ ). Physically, this suggests that the effect of Joule dissipation in the kinetic boundary layer is negligible. The transitions of the boundary layer crossover and the high Prandtl number limit from the Grossmann-Lohse theory are excluded in the present low-Pr regime. If the model were to be extended to higher Prandtl numbers, these transitions could be easily reintroduced. The revised model equations satisfactorily reproduce experimental heat transport data for liquid metals at  $\text{Pr} \sim 0.025$ . Additional experimental data at different Prandtl numbers, for example in liquid sodium with  $\text{Pr} \sim 0.005$ , would be desirable to further verification of the model. The momentum transport predictions agree less well with experimental results. This shows that the suppression of turbulence by the magnetic field cannot be fully reproduced by the Grossmann-Lohse ansatz. Together with a more rigorous treatment of the weakly non-linear and laminar regimes this is a major challenge for this mean-field theory and should be considered in future investigations.

## ACKNOWLEDGMENTS

The author would like to thank Jrg Schumacher for insightful discussions and helpful suggestions. This work was supported by the Deutsche Forschungsgemeinschaft with grant no. GRK 1567.

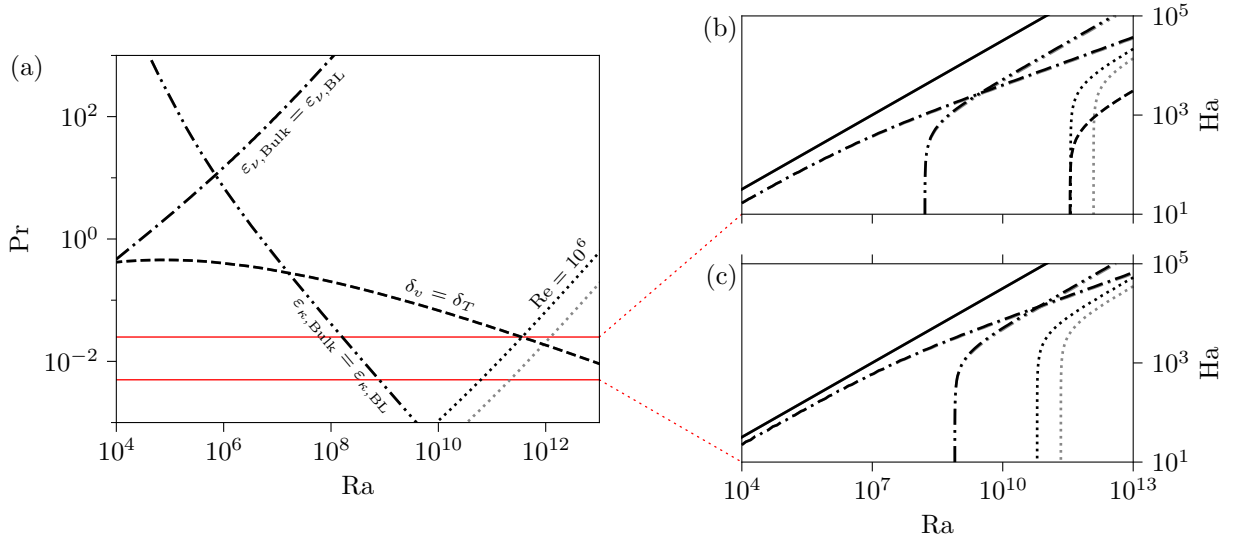


Figure 6. Phase diagrams of the model with onset transition and re-scaled parameters (A.3). Regime boundaries are plotted as black lines with the same line styles as in figure 5. The corresponding regime boundaries with the un-scaled parameters (13) and (16) are replotted from figure 5 as gray lines. (a)  $(\text{Ra}, \text{Pr})$  phase diagram at  $\text{Ha} = 0$ . (b) and (c)  $(\text{Ra}, \text{Ha})$  phase diagram at  $\text{Pr} = 0.025$  and  $\text{Pr} = 0.005$ , respectively.

### Appendix: Reynolds number re-scaling

The model equations (10) and (11) are invariant under the transformations

$$\begin{aligned} \text{Re} &\rightarrow \beta \text{Re}, & c_1 &\rightarrow \beta^{-3} c_1, & c_2 &\rightarrow \beta^{-2} c_2, & c_3 &\rightarrow \beta^{-2} c_3, \\ c_4 &\rightarrow \beta^{-2} c_4, & c_5 &\rightarrow \beta^{-1} c_5, & c_6 &\rightarrow \beta^{-1/2} c_6, & a &\rightarrow \beta^{1/2} a \end{aligned} \quad (\text{A.1})$$

for any  $\beta \in \mathbb{R}$ . This means that the Reynolds number can be re-scaled by an arbitrary factor without affecting the result of the Nusselt number. In [17] it was shown, that the Reynolds number of the GL theory under-predicts the experimental Reynolds number  $\text{Re}_{\text{LSC}}$  based on the velocity of the large-scale circulation (LSC), i.e., the convective wind. To adapt  $\text{Re}$  of the model to the experimental data, the factor  $\beta$  is determined by

$$\beta = \frac{\text{Re}_{\text{LSC}}}{\text{Re}(\text{Ra}, \text{Ha}, \text{Pr})}, \quad (\text{A.2})$$

where  $\text{Re}$  is calculated with model parameters (13) and (16) at the point  $(\text{Ra}, \text{Ha}, \text{Pr})$  at which  $\text{Re}_{\text{LSC}}$  was measured (in [17]  $\text{Ha} = 0$  and  $\text{Pr} = 0.029$  for all measurements). The average result is  $\beta = 1.81$  and the resulting re-scaled model parameters are

$$c_1 = 0.233, \quad c_2 = 2.26, \quad c_3 = 0.0137, \quad c_4 = 2.30 \times 10^{-18}, \quad c_5 = 0.0139, \quad c_6 = 0.362, \quad a = 1.24. \quad (\text{A.3})$$

While the Nusselt number is unchanged, some of the regime boundaries are affected. Figure 6 shows the regime boundaries of the re-scaled model (black lines) in comparison to the un-scaled model (gray lines, re-plot of the black lines in figure 5). The BL crossover and DR contribution crossovers are unchanged, as they are invariant under the transformations (A.1) as well. However, the  $\text{Re} = 10^6$  boundary is shifted to smaller  $\text{Ra}$ . As a result, for  $\text{Pr} = 0.025$  (figure 6(c)) the BL crossover and  $\text{Re} = 10^6$  coincidentally take place at the same  $\text{Ra}$  for  $\text{Ha} \lesssim 10^2$ .

As the Reynolds number can only be adjusted by a constant factor these re-scaled parameters are only valid for small Prandtl numbers. To get correct results for low-, intermediate- and high-Pr regimes, the GL theory would need to be revisited and revised to properly reproduce all these cases.

---

[1] P. A. Davidson, *An Introduction to Magnetohydrodynamics*, Cambridge Texts in Applied Mathematics, Vol. 25 (Cambridge University Press, Cambridge, United Kingdom, 2001).

- [2] H. K. Moffatt and E. Dormy, *Self-Exciting Fluid Dynamos*, Cambridge Texts in Applied Mathematics, Vol. 59 (Cambridge University Press, Cambridge, 2019).
- [3] D. H. Kelley and T. Weier, Fluid Mechanics of Liquid Metal Batteries, *Appl. Mech. Rev.* **70**, 020801 (2018).
- [4] T. Ihli, T. K. Basu, L. M. Giancarli, S. Konishi, S. Malang, F. Najmabadi, S. Nishio, A. R. Raffray, C. V. S. Rao, A. Sagara, and Y. Wu, Review of blanket designs for advanced fusion reactors, *Fusion Eng. Des.* **83**, 912 (2008).
- [5] T. Zürner, W. Liu, D. Krasnov, and J. Schumacher, Heat and momentum transfer for magnetoconvection in a vertical external magnetic field, *Phys. Rev. E* **94**, 043108 (2016).
- [6] S. Grossmann and D. Lohse, Scaling in thermal convection: A unifying theory, *J. Fluid Mech.* **407**, 27 (2000).
- [7] S. Chakraborty, On scaling laws in turbulent magnetohydrodynamic Rayleigh-Bénard convection, *Physica D* **237**, 3233 (2008).
- [8] K. Aujogue, A. Pothérat, I. Bates, F. Debray, and B. Sreenivasan, Little Earth Experiment: An instrument to model planetary cores, *Rev. Sci. Instrum.* **87**, 084502 (2016).
- [9] T. Takeshita, T. Segawa, J. A. Glazier, and M. Sano, Thermal turbulence in mercury, *Phys. Rev. Lett.* **76**, 1465 (1996).
- [10] S. Cioni, S. Ciliberto, and J. Sommeria, Strongly turbulent Rayleigh-Bénard convection in mercury: Comparison with results at moderate Prandtl number, *J. Fluid Mech.* **335**, 111 (1997).
- [11] J. A. Glazier, T. Segawa, A. Naert, and M. Sano, Evidence against 'ultrahard' thermal turbulence at very high Rayleigh numbers, *Nature* **398**, 307 (1999).
- [12] Y. Tsuji, T. Mizuno, T. Mashiko, and M. Sano, Mean wind in convective turbulence of mercury, *Phys. Rev. Lett.* **94**, 034501 (2005).
- [13] E. M. King and J. M. Aurnou, Magnetostrophic balance as the optimal state for turbulent magnetoconvection, *Proc. Natl. Acad. Sci. USA* **112**, 990 (2015).
- [14] R. Khalilov, I. Kolesnichenko, A. Pavlinov, A. Mamykin, A. Shestakov, and P. Frick, Thermal convection of liquid sodium in inclined cylinders, *Phys. Rev. Fluids* **3**, 043503 (2018).
- [15] T. Vogt, S. Horn, A. M. Grannan, and J. M. Aurnou, Jump rope vortex in liquid metal convection, *Proc. Natl. Acad. Sci. USA* **115**, 12674 (2018).
- [16] M. Akashi, T. Yanagisawa, Y. Tasaka, T. Vogt, Y. Murai, and S. Eckert, Transition from convection rolls to large-scale cellular structures in turbulent Rayleigh-Bénard convection in a liquid metal layer, *Phys. Rev. Fluids* **4**, 033501 (2019).
- [17] T. Zürner, F. Schindler, T. Vogt, S. Eckert, and J. Schumacher, Combined measurement of velocity and temperature in liquid metal convection, *J. Fluid Mech.* **876**, 1108 (2019).
- [18] S. Cioni, S. Chaumat, and J. Sommeria, Effect of a vertical magnetic field on turbulent Rayleigh-Bénard convection, *Phys. Rev. E* **62**, R4520 (2000).
- [19] J. M. Aurnou and P. L. Olson, Experiments on Rayleigh-Bénard convection, magnetoconvection and rotating magnetoconvection in liquid gallium, *J. Fluid Mech.* **430**, 283 (2001).
- [20] U. Burr and U. Müller, Rayleigh-Bénard convection in liquid metal layers under the influence of a vertical magnetic field, *Phys. Fluids* **13**, 3247 (2001).
- [21] T. Zürner, F. Schindler, T. Vogt, S. Eckert, and J. Schumacher, Flow regimes of Rayleigh-Bénard convection in a vertical magnetic field, *J. Fluid Mech.* **894**, A21 (2020).
- [22] W. Liu, D. Krasnov, and J. Schumacher, Wall modes in magnetoconvection at high Hartmann numbers, *J. Fluid Mech.* **849**, R2 (2018).
- [23] M. Yan, M. A. Calkins, S. Maffei, K. Julien, S. M. Tobias, and P. Marti, Heat transfer and flow regimes in quasi-static magnetoconvection with a vertical magnetic field, *J. Fluid Mech.* **877**, 1186 (2019).
- [24] Z. L. Lim, K. L. Chong, G.-Y. Ding, and K.-Q. Xia, Quasistatic magnetoconvection: Heat transport enhancement and boundary layer crossing, *J. Fluid Mech.* **870**, 519 (2019).
- [25] R. Akhmedagaev, O. Zikanov, D. Krasnov, and J. Schumacher, Turbulent convection in strong vertical magnetic field, *J. Fluid Mech.*, in press (2020).
- [26] S. Grossmann and D. Lohse, Thermal convection for large Prandtl numbers, *Phys. Rev. Lett.* **86**, 3316 (2001).
- [27] S. Grossmann and D. Lohse, Prandtl and Rayleigh number dependence of the Reynolds number in turbulent thermal convection, *Phys. Rev. E* **66**, 016305 (2002).
- [28] S. Grossmann and D. Lohse, Fluctuations in turbulent Rayleigh-Bénard convection: The role of plumes, *Phys. Fluids* **16**, 4462 (2004).
- [29] S. Grossmann and D. Lohse, Thermal convection in small Prandtl number liquids: Strong but ineffective, *AIP Conf. Proc.* **1076**, 68 (2008).
- [30] R. J. A. M. Stevens, E. P. van der Poel, S. Grossmann, and D. Lohse, The unifying theory of scaling in thermal convection: The updated prefactors, *J. Fluid Mech.* **730**, 295 (2013).
- [31] S. Bhattacharya, A. Pandey, A. Kumar, and M. K. Verma, Complexity of viscous dissipation in turbulent thermal convection, *Phys. Fluids* **30**, 031702 (2018).
- [32] S. Chandrasekhar, *Hydrodynamic and Hydromagnetic Stability*, 3rd ed. (Dover Publications, Inc., New York, 1961).
- [33] J. D. Scheel and J. Schumacher, Global and local statistics in turbulent convection at low Prandtl numbers, *J. Fluid Mech.* **802**, 147 (2016).
- [34] J. D. Scheel and J. Schumacher, Predicting transition ranges to fully turbulent viscous boundary layers in low Prandtl number convection flows, *Phys. Rev. Fluids* **2**, 123501 (2017).
- [35] F. H. Busse, Non-linear properties of thermal convection, *Rep. Prog. Phys.* **41**, 1929 (1978).
- [36] M. Breuer, S. Wessling, J. Schmalzl, and U. Hansen, Effect of inertia in Rayleigh-Bénard convection, *Phys. Rev. E* **69**, 026302 (2004).

- [37] J. Schumacher, P. Götzfried, and J. D. Scheel, Enhanced enstrophy generation for turbulent convection in low-Prandtl-number fluids, *Proc. Natl. Acad. Sci. USA* **112**, 9530 (2015).